WILEY-VCH

Mixed spacer cation stabilization of blue-emitting n=2 Ruddlesden-Popper organic-inorganic halide perovskite films

Tik Lun Leung, Ho Won Tam, Fangzhou Liu, Jingyang Lin, Alan Man Ching Ng, Wai Kin Chan, Wei Chen, Zhubing He, Ivor Lončarić, Luca Grisanti, Chao Ma, Kam Sing Wong, Ying Suet Lau, Furong Zhu, Željko Skoko, Jasminka Popović,* and Aleksandra B. Djurišić*

T. L. Leung, H. W. Tam, Dr. F. Z. Liu, J. Y. Lin, Prof. A. B. Djurišić
Department of Physics, The University of Hong Kong, Pokfulam Road, Hong Kong
E-mail: dalek@hku.hk

Dr. A. M. C. Ng
Department of Physics, Southern University of Science and Technology, No. 1088, Xueyuan Road, Shenzhen, Guangdong, China

Prof. W. K. Chan
Department of Chemistry, The University of Hong Kong, Pokfulam Road, Hong Kong

W. Chen, Dr. Z. B. He
Department of Materials Science and Engineering, Shenzhen Key Laboratory of Full Spectral Solar Electricity Generation (FSSEG), Southern University of Science and Technology, No. 1088, Xueyuan Road, Shenzhen, China

Dr. I. Lončarić, Dr. L. Grisanti
Division of Theoretical Physics, Condensed Matter and Statistical Physics Group, Ruđer Bošković Institute, Bijenička 54, Zagreb, Croatia

C. Ma, Prof. K. S. Wong
Department of Physics, The Hong Kong University of Science and Technology, Clearwater Bay, Hong Kong

Y. S. Lau, Prof. F. R. Zhu
Department of Physics, Research Centre of Excellence for Organic Electronics and Institute of Advanced Materials, Hong Kong Baptist University, Kowloon Town, Hong Kong

Prof. Ž. Skoko
Department of Physics, Faculty of Science, University of Zagreb, Bijenička 32, Zagreb, Croatia

Dr. J. Popović
Division of Materials Physics, Laboratory for Synthesis and Crystallography of Functional Materials, Ruđer Bošković Institute, Bijenička 54, Zagreb, Croatia
E-mail: jpopovic@irb.hr

Keywords: Ruddlesden-Popper, quasi-2D perovskites, perovskite light-emitting diodes, blue emission

Abstract

Ruddlesden-Popper halide perovskite (RPP) materials are of significant interest for light emitting devices since their emission wavelength can be controlled by tuning the number of layers n, resulting in improved spectral stability compared to mixed halide devices. However, RPP films typically contain phases with different n and the low n phases tend to be unstable upon exposure to humidity, irradiation, and/or elevated temperature which hinders the achievement of pure blue emission from $n=2$ films. In this work, two spacer cations are used to form a RPP film with mixed cation bilayer and high $n=2$ phase purity, improved stability and brighter light emission compared to single spacer cation RPP. The stabilization of $n=2$ phase is attributed to favorable formation energy, reduced strain and reduced electron-phonon coupling compared to the RPP films with only one type of spacer cation. Using this approach, pure blue LEDs with CIE coordinates of (0.156, 0.088) and excellent spectral stability are achieved.

Introduction

Halide perovskite LEDs, including those based on Ruddlesden-Popper perovskites (RPP), have been attracting increasing attention.[1-4] RPP have a general formula $R_2A_{n-1}B_nX_{3n+1}$, where R^+ is the bulky amine spacer cation, A^+ is an organic cation, B^{2+} is a metal cation, X^- is a halide anion and n is the number of perovskite layers between the spacer cations. RP perovskites have been extensively studied[5-32] since the choices of R and n enable wider tunability of properties compared to 3D perovskites ABX_3. Emission tuning by changing n instead of using halide mixtures enables improved color stability compared to mixed halide LEDs which commonly exhibit peak shifts with time and/or bias due to phase segregation.[3,4,28] However, while exfoliated RPP single crystals exhibit clear dependence of properties on the number of layers n, thin films typically consist of a mixture of phases with different n[1,10,17,21,23,25,26] and the phase pure films (achieved for one spacer cation via melt-processing instead of commonly used spin-coating) have been scarce.[31] The existence of multiple n phases is undesirable for LED applications since it can lead to emission peak shift with increasing bias.[23] Thus, considerable efforts have been made to control the phase composition and layer orientation in RPP thin films, especially those containing common spacer cations such as butylammonium (BA)[6-8,10,24,29,30] and phenethylammonium (PEA).[14,19,20,23,30] Despite these efforts, the differences in behavior (processability, stability and emission efficiency) of the RPP with BA and PEA spacer cations are not well understood, and the blue emitting RPP typically contain multiple peaks in either absorption or emission spectra,[21,23,25,26,28] indicating that phase purity has not been achieved. Furthermore, energy funneling phenomenon,[1,17,20] which involves energy transfer from lower n (higher energy) to higher n (lower energy) domains resulting in a brighter, but red shifted emission, represents further difficulty in obtaining pure blue emission from $n=2$ RPP emitters. Therefore, green emission[21] or at best sky blue (~490 nm) emission,[23] is usually obtained in LEDs even for

predominant $n=2$ composition of the film[21] and suppressed formation of $n=1$ phase using processing additives.[23] Consequently, there have been only a few reports on RPP LEDs with deep blue to pure blue emission (center emission at ~450-465 nm), and the reported efficiencies have been low (~10^{-3}% for devices emitting <460 nm,[4,21] and 0.15% recently achieved for ~465 nm, $<n>=3$,[28]). Experimental efforts to obtain pure phase $n=2$ films with pure blue emission are further hampered by inadequate theoretical understanding of the RPP formation and the effects of the spacer cation on the material properties, in particular those which can affect the emission efficiency, such as electron-phonon coupling[13] and strain relaxation[33] which affects trap density. Formation energies, bandgaps, etc. reported until today have been calculated by density functional theory (DFT) at 0 K.[5,13,23] Furthermore, electron-phonon coupling in RPP has so far been (only) indirectly addressed, either by means of structural arguments,[34] or based on average displacements through molecular dynamics.[13] Performing DFT calculations at room temperature enables improved understanding of the effect of spacer cation on RPP properties that can be compared to real experimental conditions and offers an insight into the feasibilty of stabilization of $n=2$ perovskite phase by the alternative mixed-cation approach.

In this work, high phase purity $n=2$ films with improved light emission in deep-blue region and improved ambient and thermal stability are achieved in a RPP material which incorporates two different spacer cations (BA and PEA) forming a mixed bilayer, which embodies the processing advantages of BA, as well as high brightness and improved ambient stability of PEA. While the addition of a second spacer cation in solar cells based on higher n perovskites can lead to reduced recombination losses,[35-37] improved morphology and crystal orientation,[37] improved ambient stability[35] and reduced phase segregation under laser irradiation,[36] the underlying mechanism has not been understood. To elucidate reasons responsible for the observed phenomena, we performed comprehensive theoretical computations, taking advantage of DFT *ab-initio* molecular dynamics, including van der

Waals forces, to improve the evaluation of formation energies and quantify electron-phonon (e-ph) couplings. Formation energies are obtained from NVT ensemble molecular dynamics at 300 K of each product and reactant, and therefore, in contrast to common static T=0 K approaches, room temperature contributions are also included. Estimation of e-ph couplings is obtained from Fourier transform of time dependent band gaps in NVE ensemble molecular dynamics (see Methods for more details). Theoretical simulations are combined with comprehensive experimental characterisations of the RPP films with pure BA, PEA and mixed BA,PEA spacer cations, and LEDs based on phase pure n=2 films are demonstrated. In terms of efficiency both $(BA_{0.5}PEA_{0.5})_2MAPb_2Br_7$ and $BA_2MAPb_2Br_7$ devices exhibit comparable values of the order of 10^{-2}% which is an order of magnitude higher compared to a previous report with multiple emission peaks for $BA_2MA_{n-1}Pb_nBr_{3n+1}$.[21] However, due to the thermal instability of n=2 phase, EL of pure BA based devices is shifted to 468 nm, resulting in a sky-blue emission with CIE coordinates of (0.132, 0.104). In the case of $(BA_{0.5}PEA_{0.5})_2MAPb_2Br_7$ devices, the improved stability of n=2 phase results in emission centered at 456 nm with CIE coordinates (0.156, 0.088) which are very close to the NTSC pure blue standard (0.14, 0.08).

Results and Discussion

The results of DFT calculations are summarised in **Figure 1**, **Tables S1, S2, S3** and **Figure S1**, Supporting Information. The calculations show that the formation energies of both $BA_2MAPb_2Br_7$ and mixed cation $(BA_{0.5}PEA_{0.5})_2MAPb_2Br_7$ exhibit the same trend (**Figure 1a)**; in both cases n=2 phase is characterized with the lowest formation energy, compared to n=1 and n=3, indicating that the crystallization of n=2 phase should be possible without the formation of any lower or/and higher n impurities. From an experimental point of view, an appearance of higher n would have been especially bothersome since it often leads to the redshift in emission due to energy funneling. Nevertheless, the calculations showed that the formation energy of n=3 mixed phase is much higher compared to n=2. While this does not

preclude the formation of $n=1$ and $n=3$ phases under some experimental conditions (especially taking into account the formation of solvent intermediates, solubility differences and their effect on crystallization), it is a clear indication that there exist conditions under which it is possible to obtain phase-pure films. On the other hand, our theoretical estimation suggests that a mixture of phases should be expected in the case of PEA-based perovskite. **Figure 1a** shows that $n=1$ phase has the lowest formation energy but we can notice that the formation energies for different values of n are also quite similar. Our calculations agree with reported trend for the experimentally determined energies of formation of $(BA)_2(MA)_{n-1}Pb_nI_{3n+1}$ which show that the formation energies for structures with an even number of layers are significantly more exothermic than those for odd values of n, i.e. the formation energy of $n=2$ is more negative than that of $n=1$ and $n=3$.[38]

Additionally, it is important to highlight that lower n ($n=1, 2$) RPP typically exhibit strain due to the lack of rotational degrees of freedom of surface octahedra which prevents strain relaxation.[33] Our DFT calculations, see **Figure 1b** and Table S3, show that $(BA_{0.5}PEA_{0.5})_2MAPb2Br_7$ exhibits the smallest strain, compared to pure BA and pure PEA spacer cations, which is expected to result in reduced formation of defects and enhanced light emission. Finally, as shown in **Figure 1c**, smaller e-ph coupling was found for $n=2$ BA-PEA mixed RPP, compared to pure BA and PEA, which may contribute to the emission enhancement and/or improved stability of photoluminescence and electroluminescence. As shown in Figure S1, e-ph coupling is due to low frequency vibrations of inorganic frame[32] (<200 cm^{-1}) and coupled vibrations of organic cations.

Figure 2 shows the absorption and PL spectra and XRD patterns of $BA_2MA_{n-1}Pb_nBr_{3n+1}$, $PEA_2MA_{n-1}Pb_nBr_{3n+1}$ and $(BA_{0.5}PEA_{0.5})_2MAPb2Br_7$ thin films prepared from solutions corresponding to $n=2$ stoichiometry. In the case of BA-perovskite, high phase purity of $n=2$ phase is evident from the absorption spectra as well as a prominent blue emission in the PL spectra (**Figure 2a**). Asymmetric line shape does not necessarily indicate the presence

of additional phases since it is commonly observed in $n=1$ RPPs which only have one phase, and it occurs due to strong exciton-phonon coupling.[27] The formation of pure phase BA films is also supported by the estimation of formation energy as shown in **Figure 1a**. The energies are calculated from the molecular dynamics simulations and therefore, in contrast to common static $T=0$ K approaches, room temperature contributions are also included. It can be observed that both temperature contributions as well as contributions of van der Waals forces are very significant (**Figure 1a, Table S1)** thus quite a different stability landscape would have been obtained if those contributions are marginalised. Additionally, XRD also confirmed that the only phase present is $BA_2MAPb_2Br_7$ ($n=2$) (**Figure 2d**). The structure has been refined in *Ama*2 space group exhibiting the periodicity 38.72(3) Å along the *c*-direction. The value of *c* parameter is slightly smaller, as expected due to the smaller radii of Br^-, compared to its iodine analogue $BA_2MAPb_2I_7$ reported by Stoumpos *et al.*[5]

For PEA-based RPP films prepared with solution stoichiometry corresponding to $n=2$, we observe a significant presence of the $n=1$ phase in the absorption spectra together with the excitonic features corresponding to $n=2$ and $n=3$ (**Figure 2b**). The presence of multiple n phases is common for $PEA_2MA_{n-1}Pb_nX_{3n+1}$.[17, 20, 23,30] The prominent presence of $n=1$ phase is additionally confirmed by XRD. For the full pattern decomposition shown in **Figure 2e**, the unit-cell parameters of iodide analogue[39,40] has been used as a starting structural model. The refinement showed that that *c*-parameter of PEA_2PbBr_4 amounts to 17.53(1) Å which is slightly smaller than 17.69 Å reported in the case of PEA_2PbI_4.[39] Although $n=1$ is dominant phase, the observed luminescence from PEA-based samples is green, which is attributed to energy funneling, i.e. the energy transfers to a small amount of the highest n phase. The fact that PEA sample showed the presence of $n=1-3$ phases, while the BA exclusively contains only $n=2$, is attributed to the negligible differences in the formation energies for $n=1, 2$ and 3 phases at RT in the case of PEA (**Figure 1a**). Additionally, both the T-shaped[13] and π-π stacking arrangements[41] of PEA molecules within the spacer bilayer have been considered;

computational structural relaxation favours T-shaped arrangement as minimum energy structure for n=1, while for higher n minimum energy structure contains π-π ordered PEA molecules (**Table S2**, Supporting Information). As a consequence, e-ph coupling for n=2 and n=3 is 1-order of magnitude larger than the coupling for n=1. This indicates that previously reported tremendous difference in PLQY for PEA perovskites compared to BA (17% for BA-based and 79% for PEA-based 2D perovskite)[1,13] would only hold for n=1 (excluding any contributions of energy funneling effect to the emission in films with multiple n phases).

From the absorption spectra of $(BA_{0.5}PEA_{0.5})_2MAPb_2Br_7$ shown in **Figure 2c** we can observe that, similar to BA- and opposite from PEA-based samples, we obtain high phase purity material corresponding exclusively to n=2. This is different from a previous report, where the addition of up to 60% of iso-propylammonium bromide failed to result in the formation of phase-pure PEA-based RPP.[23] Structural features of prepared mixed BA-PEA n=2 perovskite thin film have additionally been investigated by XRD as shown in **Figure 2d** and **Figure S2**. **Figure S2** shows XRD pattern of $(BA_{0.5}PEA_{0.5})_2MAPb_2Br_7$ compared to the $BA_2MAPb_2Br_7$ pattern and to the pattern calculated from published structure $PEA_2MAPb_2I_7$.[39] Ideally, one should make this comparison by using the pattern $PEA_2MAPb_2Br_7$ instead of $PEA_2MAPb_2I_7$, however in the scope of our work n=2 PEA bromide-based perovskite has not been obtained (we obtained n=1 as a dominant phase), nor is bromide-based structure known from the literature. Nevertheless, it is reasonable to assume that PEA-based bromide perovskite would show only small shifts in line positions compared to iodide analogue. From **Figure S2** it is obvious that mixed compound has indeed formed, since the XRD pattern of mixed perovskite is different compared to those of its end members (BA- and PEA-based perovskite). Additionally, significant line broadening can be noticed in XRD pattern of mixed- compared to single cation- perovskites that likely arose from the competition of the two ammonium cations to occupy the allocated positions in the perovskite lattice. Full pattern decomposition (**Figure 1f**) has been performed by using the structural model as obtained by the DFT. DFT

optimization of cell parameters as well as all atomic coordinates have been performed on the starting model that is built by considering the unit cell of PEA perovskite in which every second PEA molecule is substituted by BA molecule. Combined DFT and XRD study revealed that new mixed BA-PEA material crystallizes in a triclinic system, space group P1 with lattice parameters a=8.411(3) Å, b=8.176(2) Å, c=21.991(5) Å, α=97.37(1)°, β=100.04(2)° and γ=89.28(1)°. Determined c-parameter of $(BA_{0.5}PEA_{0.5})_2MAPb_2Br_7$ is similar to the c-parameter of parent PEA structure (22.76 Å for iodine analogue).[39] This is expected if one considers that the assembly of mixed spacer bilayer has to be dominated by the longer ammonium cation. The presence of both PEA and BA cations has also been confirmed by NMR measurements, as shown in **Figure 1g**. The molar ratio of PEA:BA:MA was calculated to be 1:1:1 which agrees with the stoichiometry of $(BA_{0.5}PEA_{0.5})_2MAPb_2Br_7$. We also investigated the composition of the films prepared with different ratio of PEA and BA. For lower PEA content (i.e. 0.25, 0.50), only n=2 excitonic feature in the absorption spectra, as shown in **Figure S3**, Supporting Information. With increased PEA content (0.75), we can observe the appearance of n=1 phase. Those findings indicate that the ratio of two cations might play a determining role in the stabilization of n=2 mixed perovskite material. While the incorporation of PEA cations leads to enhanced PL and improved thermal stability of BA-PEA perovskite compared to pure BA perovskite, once PEA content becomes too large, the stabilizing effect diminishes thus resulting in the crystallization of multiple n mixture. This behaviour is likely to be caused by the fact that PEA cation, unlike BA, is often disordered. [39] The concept of having perovskite material containing two different cations in spacer bilayer can also be demonstrated for n=1 as shown in **Figure S4**, Supporting Information. In agreement with calculated formation energies of BA_2PbBr_4 and PEA_2PbBr_4, that are lower than the formation energy of $(BA_{0.5}PEA_{0.5})_2PbBr_4$, we obtained a mixture of all three phases. Deposition method altering crystallization kinetics and favouring more rapid nucleation, such as vacuum drying, blow-drying and the use of anti solvent reduce the

proportion of BA_2PbBr_4 and PEA_2PbBr_4 phases, as shown in **Figure S5**, Supporting Information. Thus, we clearly show that mixed spacer cations lead to the formation of distinctly different crystal structure.

Our theoretical calculations also predict superior optical properties due to lower strain and lower e-ph coupling in mixed cation samples. Experimentally, we indeed obtained higher luminescence from the $(BA_{0.5}PEA_{0.5})_2MAPb_2Br_7$ compared to $BA_2MAPb_2Br_7$ films, while the films have comparable thickness (174 ± 12 nm and 185 ± 16 nm, respectively). However, luminescence intensity is also dependent on the native defects in the films, which are affected by the deposition conditions. Therefore, we performed comprehensive optimization of the film deposition conditions for $(BA_{0.5}PEA_{0.5})_2MAPb_2Br_7$ and $BA_2MAPb_2Br_7$ films, including investigating the factors known to affect crystallization and/or optical quality, such as the effects of precursor purity, solvents and/or additives used, and the use of anti solvents.[18,29,30,42-46] The details are given in Supporting Information, **Note 1** and **Figures S6-S12**.

Figures 3 and **4** clearly illustrate advantages of the utilization of $n=2$ mixed perovskite for blue-emitting applications over pure $n=2$ BA material. From the PL spectra of optimized films shown in **Figure 3a** we can observe that mixed spacer cation films exhibit higher PL intensity compared to BA sample. The enhancement of emission is also confirmed by obtained values of photoluminescence quantum yield (PLQY), $2.80\pm0.28\%$ for $(BA_{0.5}PEA_{0.5})_2MAPb_2Br_7$ thin films and $1.66\pm0.52\%$ for $BA_2MAPb_2Br_7$ thin films (averages of 5 samples each). To further characterize the samples, we performed time-resolved photoluminescence (TRPL) measurements, as shown in **Figure S13** and summarized in **Table S4**. The PL decay curves can be described with a commonly used bi-exponential decay, and the two samples exhibit similar average lifetimes τ_{avg}. From the measured PLQY and determined τ_{avg} we can estimate radiative recombination rate k_{rad} as $k_{rad}=PLQY/\tau_{avg}$.[47] The obtained results of $2.55 \cdot10^6$ s^{-1} and $5.0 \cdot10^6$ s^{-1} indicate higher radiative recombination in

$(BA_{0.5}PEA_{0.5})_2MAPb_2Br_7$ thin films, despite lower grain sizes compared to $BA_2MAPb_2Br_7$ thin films, as shown in SEM images of films on ITO substrates in **Figure S14a** and **S14b**, Supporting Information.

We also investigated environmental stability (**Figure 3 c** and **4)** and thermal stability (**Figure 4**), since those aspects have significant impact on the device applications. It is known that the emission of lead halide perovskites can shift under UV or laser irradiation in ambient, as documented in mixed halide 3D perovskites,[23] perovskite nanoplatelets,[46] and Ruddlesden-Popper perovskites.[12] Mixed perovskite films do not show any shifts of emission peak under 325 nm laser illumination when encapsulated, as shown in **Figure 3b**, similar as in the case of BA-compound shown in **Figure S15**, Supporting information. In ambient conditions, we observe red shift of the emission peak and the reduction of the emission intensity over time as shown in **Figure 3c** and **3d** for both BA- and mixed perovskite. The same behavior is also observed in $BA_2MAPb_2Br_7$ single crystals, as shown in **Figure S15**, Supporting Information. The observed behaviour upon exposure to ambient atmosphere under laser illumination is consistent with previously reported phenomena of photobleaching and transformation in n=2 MAPbBr nanoplatelets.[41] The transformation phenomenon, i.e. the appearance of features corresponding to different n values, has been attributed to humidity.[41] While the transformation is accelerated by UV illumination, the humidity also induces the change of the phase composition over time without UV illumination.[18,24] Although both samples exhibit red shift of the emission when exposed to ambient environment under UV laser illumination, the observed red shift in mixed cation films is smaller and slower compared to pure BA films. This indicates that the transformation of the films is inhibited by cation mixing, resulting in improved environmental stability.

In addition to improved ambient stability, mixed cation films also exhibit enhanced thermal stability, which is important for LED applications due to Joule heating during operation.[28] Enhanced thermal stability is also critical for successful fabrication of blue-

emitting LEDs, since the deposition of the electrodes can result in significant temperature increases. While $BA_2MAPb_2Br_7$ films already show additional peaks in both absorption (**Figure 4a**) and PL spectra (**Figure 4c**) corresponding to $n=3$ (PL) and $n=1$ (absorption) phases after annealing for 1 min., annealed $(BA_{0.5}PEA_{0.5})_2MAPb_2Br_7$ films remain stable at elevated temperatures as evidenced from **Figures 4b** and **4d**. The annealing condition (100ºC, 1 min.) has been selected to correspond to realistic device fabrication conditions, i.e. the highest temperature observed during device deposition for the duration of the deposition of that particular layer. We found that the sample remained at room temperature (~24ºC) during TPBI deposition (~20 mins). However, electrode deposition resulted in the increase of substrate temperature, with the highest temperatures reaching ~61ºC for Al (~6 min deposition), 70ºC for Cs_2CO_3 (~10 min deposition) and ~95ºC for LiF (~1 min deposition). This leads to emission peak shifts, as illustrated in **Figure 5**. It should be noted that the PL spectrum of the devices also exhibits similar shift compared to the PL spectrum of the films before the ETL and electrode deposition, which confirms that the changes originate from the thermal instability of BA-based perovskite, in agreement with observed changes after annealing. Such pronounced red shifts of EL spectra compared to PL spectra, as observed for BA film, are typically observed in films with inferior ambient and thermal stability, while mixed spacer cation films can retain blue emission.

Due to their promising optical properties, we have investigated the application of optimized $(BA_{0.5}PEA_{0.5})_2MAPb_2Br_7$ films to obtain deep-blue LEDs. Device architecture is shown in **Figure 6**, while SEM of the $(BA_{0.5}PEA_{0.5})_2MAPb_2Br_7$ and $BA_2MAPb_2Br_7$ on the hole transport layer (HTL) and I-V curves of hole-only devices are shown in **Figure S14c, S14d** and **S16**, Supporting Information. Both BA-PEA and pure BA samples exhibit comparable efficiency of the order of 10^{-2}% (**Figure 6b** and **6c**) and in both cases the EQE exhibited a roll-off, which is common in perovskite LEDs,[21,23,26,28] and it can be attributed to non-radiative defects[28] and Auger recombination.[26] The efficiency could likely be further

improved with optimization of the film morphology on the HTL, since the films on ITO exhibit lower surface roughness and fewer defects (aggregates, pinholes). It can be seen that $BA_2MAPb_2Br_7$ devices exhibit a maximum EQE of 0.026% (average value of 0.013±0.009% for five devices). However, due to inherent instability of BA-based films when exposed to elevated temperature during electrode deposition in LED fabrication, the EL emission peak has shifted to 468 nm, with corresponding CIE coordinates of (0.132, 0.104). The significant peak shift between PL (pure blue) and EL (sky blue) spectra of the films can be clearly observed in **Figure 7a**. In contrast, mixed cation devices exhibit a very small shift between PL and EL spectra, as shown in **Figure 7b**, and pure blue emission is obtained in both cases. Consequently, the peak position of mixed BA-PEA device is centered at 456 nm with CIE coordinates of (0.156, 0.088) which is very close to the NTSC blue standard of (0.14, 0.08). The maximum EQE of $(BA_{0.5}PEA_{0.5})_2MAPb_2Br_7$ is to 0.015% (average value of 0.012%±0.001 which is two times higher than previously reported blue emission LED from the BA-based RPP exhibiting multiple peaks with dominant emission at ~450 nm, poor spectral stability and the efficiency of 0.0054%[21] indicating significant progress towards the achievement of pure blue emission in a quasi-2D RPP emitter without halogen mixing. Moreover, despite the fact that high spectral stability in blue-emitting perovskite LEDs has been scarce,[23,28] both of our devices exhibit excellent spectral stability over time (**Figure 7 c and 7d**) as well as bias voltage (**Figure 7 e and 7f**). Furthermore, both BA and BA-PEA based devices exhibit exponential decay of emission intensity, as shown in **Figure S17**, Supporting Information. The obtained time constants τ and the corresponding T_{50} are τ=47.3 s and T_{50}=70.6 for BA-based device, and τ=100.7 s and T_{50}=91.4 for BA-PEA based device, illustrating the improved stability of mixed cation film. The obtained value of T_{50} of ~1.5 min is comparable to that typically reported for blue perovskite LEDs (several minutes, longer T_{50} for longer wavelength).[23,28] Finally, it should also be noted that the mixed cation approach is not only applicable to BA-PEA cation combination, but also to other cations. The

generalization of mixed spacer cation approach for stabilization of $n=2$ phase is demonstrated for different spacer cation combinations (benzylammonium (BZA) and BA, 4-fluoro-phenethylammonium (FPEA) and BA), as shown in **Figure S18**, Supporting Information.

Conclusions

We demonstrate the use of two different spacer cations to obtain an RPP with a mixed bilayer which exhibits distinct advantages over RPP materials with a single spacer cation, in terms of phase purity, light emission intensity, as well as ambient and thermal stability. Based on comprehensive DFT calculations including *ab-initio* molecular dynamics, we attribute improved properties to more favorable formation energy of $n=2$ phase, lower strain and lower e-ph coupling. The approach is applicable to other combinations of spacer cations, although the optimization of deposition conditions can be needed to enhance phase purity.

Materials and Methods

Materials: Phenethylammonium bromide (PEABr), n-butylammonium bromide (BABr), methylammonium bromide (MABr), benzylammonium bromide (BZABr), 4-fluorophenethylammonium bromide (FPEABr) were purchased from Greatcell Solar Materials. Lead bromide ($PbBr_2$, 99.998%), hydrobromic acid (HBr, 48% w/w aq. soln.), acetonitrile (ACN, anhydrous, 99.8+%), iso-propanol (IPA, anhydrous, 99.5+%), N,N-dimethylformamide (DMF, anhydrous, 99.9%), dimethyl sulfoxide (DMSO, anhydrous, 99.9%), 18-crown-6 (99%) and trioctylphosphine oxide (TOPO, 98%) were bought from Alfa Aesar. Lead bromide (≥98%), chlorobenzene (anhydrous, 99.8%), methyl acetate (MAc, anhydrous, 99.5%), nickel(II) acetate tetrahydrate ($Ni(Ac)_2 \cdot 4H_2O$, 99.998%), and ethanolamine (≥99%) were purchased from Sigma Aldrich. Poly(9-vinylcarbazole) (PVK), 1,3,5-Tris(1-phenyl-1Hbenzimidazol-2-yl)benzene (TPBi, >99.5%) and cesium carbonate (Cs_2CO_3, >99.994%) were purchased from Luminescence Technology Corp. Hexafluorotetracyanonaphthoquinodimethane (F6TCNNQ, 99%) was purchased from Shanghai Da Ran Chemicals. 18-crown-6 was recrystallized from ACN before use. All

chemicals were used without further treatment unless otherwise specified. All solutions used for spin-coating were filtered with 0.45 μm PTFE filter.

Preparation of BA$_2$MAPb$_2$Br$_7$ single crystal: BA$_2$MAPb$_2$Br$_7$ single crystal was prepared following a previously reported method.[5] PbBr$_2$ (10 mmol) was first dissolved in HBr (15 ml) solution at 90 °C. MABr (5 mmol) and BABr (7 mmol) were then added into the hot solution, resulting in a readily formed orange precipitate. After stirring overnight, the precipitate was completely dissolved. Yellow rectangular-shaped plate was formed while the solution was cooled slowly to room temperature. The obtained crystal was cleaned with acetic acid and dried in vacuum oven at 40 °C for overnight.

Preparation of quasi-2D perovskite film: Indium tin oxide (ITO) /glass) substrates were cleaned sequentially by sonication in detergent, water, acetone and ethanol, followed by UV ozone treatment. Perovskite precursor solution was prepared by dissolving stoichiometric amounts of precursors in DMF. For example, precursor solution of BA$_2$MAPb$_2$Br$_7$ was obtained by dissolving PbBr$_2$ (0.4 mmol, 146.8 mg), BABr (0.4 mmol, 61.8 mg) and MABr (0.2 mmol, 22.4 mg) in DMF (1 ml) at room temperature. Precursor solution of PEA$_2$MAPb$_2$Br$_7$ was prepared by replacing BABr with PEABr while precursor solution of PEA-BA mixed perovskite was prepared by mixing desired ratio of PEA and BA based precursor solutions. Perovskite films were deposited on ITO/glass substrates via spin-coating with a two-step approach of 1000 rpm for 10s and 4000 rpm for 45s. The film was then vacuum dried for 10 min before further treatment or characterization. All processes were conducted in an argon filled glovebox.

Characterization of quasi-2D perovskite film: All optical measurements were performed with perovskite films encapsulated by quartz plates except for the stability test of the perovskite samples. Steady state PL spectra were obtained by PDA-512 USB (Control Development Inc.) Fiberoptic Spectrometer with a HeCd laser (325 nm) as the excitation source. A comparison technique was used to estimate the PLQY of the encapsulated perovskite films.

First, PL of these samples and the standard reference were measured in the same condition at the same alignment, with a He-Cd 325nm continuous wave laser as the excitation source. In addition, incident power, reflected power, and transmitted power of the laser were measured by a calibrated photodiode power meter from Newport to determine the real absorption of the samples. The PLQY of the perovskite films was then calculated by comparing their PL intensity and absorption to the standard reference. The external PLQY of the standard reference sample was acquired with a home-made setup. A He-Cd 325nm continuous wave laser was used as the excitation source and the emission signals were detected using a calibrated integrating sphere (Labsphere) together with an Ocean Optics USB2000 spectrometer. The data acquisition and result calculation followed the protocol previously reported.[48] Absorption spectra of the perovskite samples were measured with Cary 50 UV-Vis spectrometer (Agilent Technologies). Film XRD patterns of the perovskite samples were collected with Bruker AXS D8 Advance X-Ray Diffractometer and Rigaku SmartLab 9kW X-ray Diffractometer with Cu Kα radiation. Morphology of the perovskite films was characterized using a Hitachi S-4800FEG Scanning Electron Microscope. ^{1}H-NMR spectrum was measured with a Bruker Advance 600 Fourier-transform NMR spectrometer with the perovskite samples dissolved in DMSO-d6. Time correlated single photon counting (TCSPC) was used to study the time dependent PL. A frequency doubled (400 nm) 100 femtosecond Ti:Sapphire oscillator (Coherent Mira 900) operating at a 1 MHz repetition rate was focused down to a spot size of ~100 μm to excite the sample. PL was collimated by an achromatic lens and focused onto the monochromator (Acton Spectrapro 275) slit. The PL was dispersed from a 1200 line/mm grating onto a single photon detector (Becker & Hickl DCC-100) to carry out the TCSPC measurements. Dynamic Light Scattering (DLS) analysis was obtained with the use of Zetasizer HS3000. Sample was loaded into a quartz cuvette and encapsulated with UV epoxy.

Device fabrication and characterization: Patterned ITO/glass substrates were cleaned as previously described. NiO_x thin films were prepared following a procedure previously reported.[49] Briefly, NiO_x sol-gel solution was prepared by dissolving $Ni(Ac)_2 \cdot 4H_2O$ (0.2 mmol) and ethanolamine (0.2 mmol) in IPA (1 ml) at 70 °C overnight. The sol-gel solution was spin-coated on ITO/glass substrates at 3000 rpm for 30s, followed by annealing at 275 °C for 1 h in air. F6TCNNQ solution (0.2 mg/mL in ACN) was then spin-coated on NiO_x at 4000 rpm for 60s followed by annealing overnight at 80°C. PVK solution (5 mg/ml in CB) was spin-coated on NiO_x/F6TCNNQ at 3000 rpm for 30s and annealed at 70°C for 30 min. Perovskite films were deposited on O_2 plasma treated PVK layer as described above. TOPO solution (1 mg/ml in MAc) was further spin-coated on perovskite layer for surface passivation. TPBi, Cs_2CO_3 and Al were thermally evaporated through a shadow mask with thickness of 40 nm, 1 nm, and 100 nm respectively. The active area was calculated to be 0.06 cm^2. The performance of the perovskite LEDs was characterized with a programmable Keithley model 2420 power source and a Photoresearch PR-655 spectrometer. EL spectra were recorded by fiberoptic spectrometer PDA-512 USB (Control Development Inc.) and PR655 spectrometer.

Theoretical Calculations: For static DFT calculations, we used an accurate plane-wave basis set code Quantum Espresso[50,51] with the GBRV pseudopotentials[52] and vdW-DF-cx[53,54] exchange-correlation functional. The plane wave basis set cutoff is 680 eV and first Brillouin zone is sampled by the Monkhorst-Pack k-point mesh with density of 5 Å. In each calculation unit cell and atoms were relaxed until the change in the total energy was <1 meV, forces on each atom were smaller than 0.02 eV/Å, and pressure was <0.5 kbar. Strain compared to 3D perovskite was calculated based on relaxed cells. Formation energy at T=0 was calculated from DFT energies of perovskites and of each reactant component as:

$$E_{form} = E(R_1 R_2 MA_{n-1} Pb_n Br_{3n+1}) - E(R_1 Br) - E(R_2 Br) - (n-1)E(MABr) -$$

$$nE(PbBr_2), \quad (1)$$

where E is DFT energy, and R is BA or PEA. We list all DFT optimized crystal structures in Supplementary Data. To reduce computational cost, for molecular dynamics simulations we used CP2K code[55] with PBE+D3[56,57] exchange-correlation functional. For each system we have reoptimized coordinates, run NVT ensemble molecular dynamics[58] at 300 K for 3 ps with 1 ps equilibration and NVE dynamics for 5 ps. From average potential energy in NVT ensemble we subtracted potential energy of reoptimized structure. We add these energies to each component in equation (1) to obtain energy of formation at T=300 K. This approximately correspond to a Helmholtz free formation energy, as it contains effectively thermal and entropic contributions from NVT simulations (except for zero-point energy corrections).

From NVE dynamics we extracted time dependent band gaps. Fourier transform of these time series were calculated and represented *via* scipy modules (signal.periodograms, scaling='density'), and by their integration we obtained an estimation of electron-phonon couplings.

Supporting Information
Supporting Information is available from the Wiley Online Library or from the author.

References

[1] Z. Chen, Y. Guo, E. Wertz, J. Shi, *Adv. Mater.* **2018**, *30*, 1803514.

[2] J. Hu, L. Yan, W. You, *Adv. Mater.* **2018**, *30*, 1802041.

[3] L. N. Quan, F. P. Garcia de Arquer, R. P. Sabatini, E. H. Sargent, *Adv. Mater.* **2018**, *30*, 1801996.

[4] N. K. Kumawat, X. K. Liu, D. Kabra, F. Gao, *Nanoscale* **2019**, *11*, 2109.

[5] C. C. Stoumpos, D. H. Cao, D. J. Clark, J. Young, J. M. Rondinelli, J. I. Jang, J. T. Hupp, M. G. Kanatzidis, *Chem. Mater.* **2016**, *28*, 2852.

[6] X. Zhang, R. Munir, Z. Xu, Y. C. Liu, H. H. Tsai, W. Y. Nie, J. B. Li, T. Q. Niu, D. M. Smilgies, M. G. Kanatzidis, A. D. Mohite, K. Zhao, A. Amassian, S. Z. (F.) Liu, *Adv. Mater.* **2018**, *30*, 1707166.

[7] D. H. Cao, C. C. Stoumpos, O. K. Farha, J. T. Hupp, M. G. Kanatzidis, *J. Am. Chem. Soc.* **2015** *137*, 7843.

[8] X. Q. Zhang, G. Wu, S. D. Yang, W. F. Fu, Z. Q. Zhang, C. Chen, W. Q. Liu, J. L. Yan, W. T. Yang, H. Z. Chen, *Small* **2017**, *13*, 1700611.

[9] N. R. Venkatesan, J. G. Labram, M. L. Chabinyc, *ACS Energy Lett.* **2018**, *3*, 380.

[10 L. Yan, J. Hu, Z. Guo, H. Chen, M. F. Toney, A. M. Moran, W. You, *ACS Appl. Mater. Interfaces* **2018**, *10*, 33187.

[11] P. Vashishtha, M. Ng, S. B. Shivarudraiah, J. E. Halpert, *Chem. Mater.* **2019**, *31*, 83.

[12] K. Leng, I. Abdelwahab, I. Verzhbitskiy, M. Telychko, L. Chu, W. Fu, X. Chi, N. Guo, Z. Chen, Z. Chen, C. Zhang, G. H. Xu, J. Lu, M. Chhowalla, G. Eda, K. P. Loh, *Nature Mater.* **2018**, *17*, 908.

[13] X. Gong, O. Voznyy, A. Jain, W. Liu, R. Sabatini, Z. Piontkowsky, G. Walters, G. Bappi, S. Nokhrin, O. Bushuyev, M. Yuan, R. Comin, D. McCamant, S. O. Kelley, E. H. Sargent, *Nature Mater.* **2018**, *17*, 550.

[14] X. Zhang, G. Wu, W. Fu, M. Qin, W. Yang, J. Yan, Z. Zhang, X. Lu, H. Chen, *Adv. Energy Mater.* **2018**, *8*, 1702498.

[15] W. Peng, J. Yin, K. T. Ho, O. Ouellette, M. D. Bastiani, B. Murali, O. E. Tall, C. Shen, X. H. Miao, J. Pan, E. Alarousu, J. H. He, B. S. Ooi, O. F. Mohammed, E. Sargent, O. M. Bakr, *Nano Lett.* **2017**, *17*, 4759.

[16] J. Byun, H. Cho, C. Wolf, M. Jang, A. Sadhanala, R. H. Friend, H. Yang, T. W. Lee, *Adv. Mater.* **2016**, *28*, 7515.

[17] M. Yuan, L. N. Quan, R. Comin, G. Walters, R. Sabatini, O. Voznyy, S. Hoogland, Y. Zhao, E. M. Beauregard, P. Kanjanaboos, Z. Lu, D. H. Kim, E. H. Sargent, *Nat. Nanotechnol.* **2016**, *11*, 872.

[18] Y. T. Zou, Q. Huang, Y. G. Yang, M. Y. Ban, S. Y. Li, Y. J. Han, T. Wu, Y. S. Tan, X. Y. Gao, T. Song, B. Q. Sun, *Adv. Mater. Interfaces* **2018**, *5*, 1801030.

[19] W. Fu, J. Wang, L. Zuo, K. Gao, F. Liu, D. S. Ginger, A. K. Y. Jen, *ACS Energy Lett.* **2018**, *3*, 2086.

[20] L. N. Quan, Y. Zhao, F. P. G. deArquer, R. Sabatini, G. Walters, O. Voznyy, R. Comin, Y. Li, J. Z. Fan, H. Tan, J. Pan, *Nano Lett.* **2017**, *17*, 3701.

[21] D. N. Congreve, M. C. Weidman, M. Seitz, W. Paritmongkol, N. S. Dahod, W. A. Tisdale, *ACS Photonics* **2017**, *4*, 476.

[22] P. Cai, X. Wang, H. J. Seo, X. Yan, *Appl. Phys. Lett.* **2018**, *112*, 15.

[23] J. Xing, Y. Zhao, M. Askerka, L. N. Quan, X. Gong, W. Zhao, J. Zhao, H. Tan, G. Long, L. Gao, Z. Yang, O. Voznyy, J. Tang, Z. H. Lu, Q. Xiong, E. H. Sargent, *Nat. Commun.* **2018**, *9*, 3541.

[24] C. Stoumpos, C. M. M. Soe, H. Tsai, W. Nie, J. C. Blancon, D. H. Cao, F. Liu, B. Traoré, C. Katan, J. Even, A. D. Mohite, M. G. Kanatzidis, *Chem* **2017**, *2*, 427.

[25] Q. Wang, J. Ren, X. F. Peng, X. X. Ji, X. H. Yang, *ACS Appl. Mater. Interfaces* **2017**, *9*, 29901.

[26] Z. M. Chen, C. Y. Zhang, X. F. Jiang, M. Y. Liu, R. X. Xia, T. T. Shi, D. C. Chen, Q. F. Xue, Y. J. Zhao, S. J. Su, H. L. Yip, Y. Cao, *Adv. Mater.* **2017**, *29*, 1603157.

[27] L. M. Ni, U. Huynh, A. Cheminal, T. H. Thomas, R. Shivanna, T. F. Hinrichsen, S. Ahmad, A. Sadhanala, A. Rao, *ACS Nano* **2017**, *11*, 10834.

[28] Y. Z. Jiang, C. C. Qin, M. H. Cui, T. W. He, K. K. Liu, Y. M. Huang, M. H. Luo, L. Zhang, H. Y. Xu, S. S. Li, J. L. Wei, Z. Y. Liu, H. H. Wang, G. H. Kim, M. J. Yuan, J. Chen, *Nat. Commun.* **2019**, *10*, 1868.

[29] C. J. Dahlman, R. A. DeCrescent, N. R. Venkatesan, R. M. Kennard, G. Wu, M. A. Everest, J. A. Schuler, M. L. Chabinyc, *Chem. Mater.* **2019**, *31*, 5832.

[30] R. Quintero-Bermudez, A. Gold-Parker, A. H. Proppe, R. Munir, Z. Yang, S. O. Kelly, A. Amassian, M. F. Toney, E. H. Sargent, *Nature Mater.* **2018**, *17*, 900.

[31] T. Y. Li, A. M. Zeidell, G. Findik, W. A. Dunlap-Shohl, J. Euvrard, K. Gundogdu, O. D. Jurchescu, D. B. Mitzi, *Chem. Mater.* **2019**, *31*,4267.

[32]F. Thouin, D. A. Valverde-Chàvez, C. Quarti, D. Cortecchia, I. Bargigia, D. Beljonne, A. Petrozza, C. Silva, A. R. S. Kandada, *Nature Mater.* **2018**, *18*, 349.

[33] M. Kepenekian, B. Traore, J. C. Blancon, L. Pedesseau, H. Tsai, W. Nie, C. C. Stoumpos, M. G. Kanatzidis, J. Even, A. D. Mohite, S. Tretiak, *Nano Lett.* **2018**, *18*, 5603.

[34] K. Miyata, D. Meggiolaro, M. T. Trinh, P. P. Joshi, E. Mosconi, S. C. Jones, F. De Angelis, X. Y. Zhu, "Large polarons in lead halide perovskites", *Sci. Adv.* **2017**, *3*, e1701217.

[35] S. Chen, N. Shen, L. Z. Zhang, W. G. Kong, L. Zhang, C. Cheng, B. Xu, *J. Mater. Chem. A* **2019**, *7*, 9542.

[36] M. Z. Long, T. K. Zhang, D. C. Chen, M. C. Qin, Z. F. Chen, L. Gong, X. H. Lu, F. Y. Xie, W. Xie, J. Chen, J. B. Xu, *ACS Energy Lett* **2019**, *4*, 1025.

[37] J. Qiu, Y. D. Xia, Y. T. Zheng, W. Hui, H. Gu, W. B. Yuan, H. Yu, L. F. Chao, T. T. Nou, Y. G. Yang, X. Y. Gao, Y. H. Chen, W. Huang, *ACS Energy Lett,* **2019**, *4*, 1513.

[38] C. M. M. Soe, G. P. Nagabhushana, R. Shivaramaiah, H. Tsai, W. Nie, J.-C. Blancon, F. Melkonyan, H. H. Cao, B. Traoré, L. Pedesseau, M. Kepenekian, C. Katan, J. Even, T. J. Marks, A. Navrotsky, A. D. Mohite, C. C. Stoumpos, M. G. Kanatzidis, *Proc. Natl. Acad. Sci. U. S. A.* **2019**, *116*, 58.

[39] J. Calabrese, N. L. Jones, R. L. Harlow, N. Herron, D. L. Thorn, Y. Wang, *J. Am. Chem. Soc.* **1991**, *113*, 2328.

[40] I. C. Smith, E. T. Hoke, D. Solis-Ibarra, M. D. McGehee, H. I. Karunadasa, *Angew. Chem., Int. Ed.* **2014**, *53*, 11232.

[41] A. H. Slavney, R. W. Smaha, I. C. Smith, A. Jaffe, D. Umeyama, H. I. Karundasa, *Inorg. Chem.* **2017**, *56*, 46.

[42] J. T. Tisdale, T. Smith, J. R. Salasin, M. Ahmadi, N. Johnson, A. V. Ievlev, M. Koehler, C. J. Rawn, E. Lukosi, B. Hu, *CrystEngComm* **2018**, *20*, 7818.

[43] Y. H. Hu, L. M. Spies, D. Alonso-Alvarez, P. Mocherla, H. Jones, J. Hanisch, T. Bein, P. R. F. Barnes, P. Docampo, *J. Mater. Chem. A* **2018**, *6*, 22215.

[44] F. Yang, G. Kapil, P. Zhang, Z. S. Hu, M. A. Kamarudin, T. L. Ma, S. Hayase, *ACS Appl. Mater. Interfaces* **2018**, *10*, 16482.

[45] S. Masi, F. Aiello, A. Listorti, F. Balzano, D. Altamura, C. Giannini, R. Caliandro, G. Uccello-Barretta, A. Rizzo, S. Colella, *Chem. Sci.* **2018**, *9*, 3200.

[46] S. K. Hu, C. M. Mauck, W. A. Tisdale, *Chem. Mater.* **2019**, *31*, 2486.

[47] Z. G. Xiao, R. A. Kerner, N. Tran, L. F. Zhao, G. D. Scholes, B. P. Rand, *Adv. Funct. Mater.* **2019**, *29*, 1807284.

[48] J. C. de Mello, H. F. Wittmann, R. H. Friend, *Adv. Mater.* **1997**, *9*, 230.

[49] W. Chen, Y. Zhou, L. Wang, Y. Wu, B. Tu, B. Yu, F. Liu, H.-W. Tam, G. Wang, A. B. Djurišić, L. Huang, Z. He, *Adv. Mater.* **2018**, *30*, 1800515.

[50] P. Giannozzi, S. Baroni, N. Bonini, M. Calandra, R. Car, C. Cavazzoni, D. Ceresoli, G. L Chiarotti, M. Cococcioni, I. Dabo, A. Dal Corso, S. de Gironcoli, S. Fabris, G. Fratesi, R. Gebauer, U. Gerstmann, C. Gougoussis, A. Kokalj, M. Lazzeri, L. Martin-Samos, N. Marzari, F Mauri, R. Mazzarello, S. Paolini, A. Pasquarello, L. Paulatto, C. Sbraccia, S. Scandolo, G. Sclauzero, A. P Seitsonen, A. Smogunov, P. Umari, R. M Wentzcovitch, *J. Phys. Condens. Matter* **2009**, *21*, 395502.

[51] P. Giannozzi, O. Andreussi, T. Brumme, O. Bunau, M. B. Nardelli, M. Calandra, R. Car, C. Cavazzoni, D. Ceresoli, M. Cococcioni, N. Colonna, I. Carnimeo, A. Dal Corso, S. de Gironcoli, P. Delugas, R. A. DiStasio, A. Ferretti, A. Floris, G. Fratesi, G. Fugallo, R. Gebauer, U. Gerstmann, F. Giustino, T. Gorni, J. Jia, M. Kawamura, H.-Y. Ko, A. Kokalj, E. Küçükbenli, M. Lazzeri, M. Marsili, N. Marzari, F. Mauri, N. L. Nguyen, H.-V. Nguyen, A. Otero-de-la-Roza, L. Paulatto, S. Poncé, D. Rocca, R. Sabatini, B. Santra, M. Schlipf, A. P. Seitsonen, A. Smogunov, I. Timrov, T. Thonhauser, P. Umari, N. Vast, X. Wu, S. Baroni, *J. Phys. Condens. Matter* **2017**, *21*, 395502.

[52] K. F. Garrity, J. W. Bennett, K. M. Rabe, D. Vanderbilt, *Comput. Mater. Sci.* **2014**, *81*, 446.

[53] K. Berland, C. A. Arter, V. R. Cooper, K. Lee, B. I. Lundqvist, E. Schröder, T. Thonhauser, Per Hyldgaard, *J. Chem. Phys* **2014**, *140*, 18A539.

[54] K. Berland, P. Hyldgaard, *Phys. Rev. B* **2014**, *89*, 035412.

[55] J. Hutter, M. Iannuzzi, F. Schiffmann, J. VandeVondele, *WIREs Comput Mol Sci* **2014**, *4*, 15.

[56] J. P. Perdew, K. Burke, M. Ernzerhof, *Phys. Rev. Lett.* **1996**, *77*, 3865.

[57] S. Grimme, J. Antony, S. Ehrlich, H. Krieg, *J. Chem. Phys.* **2010**, *132*, 154104.

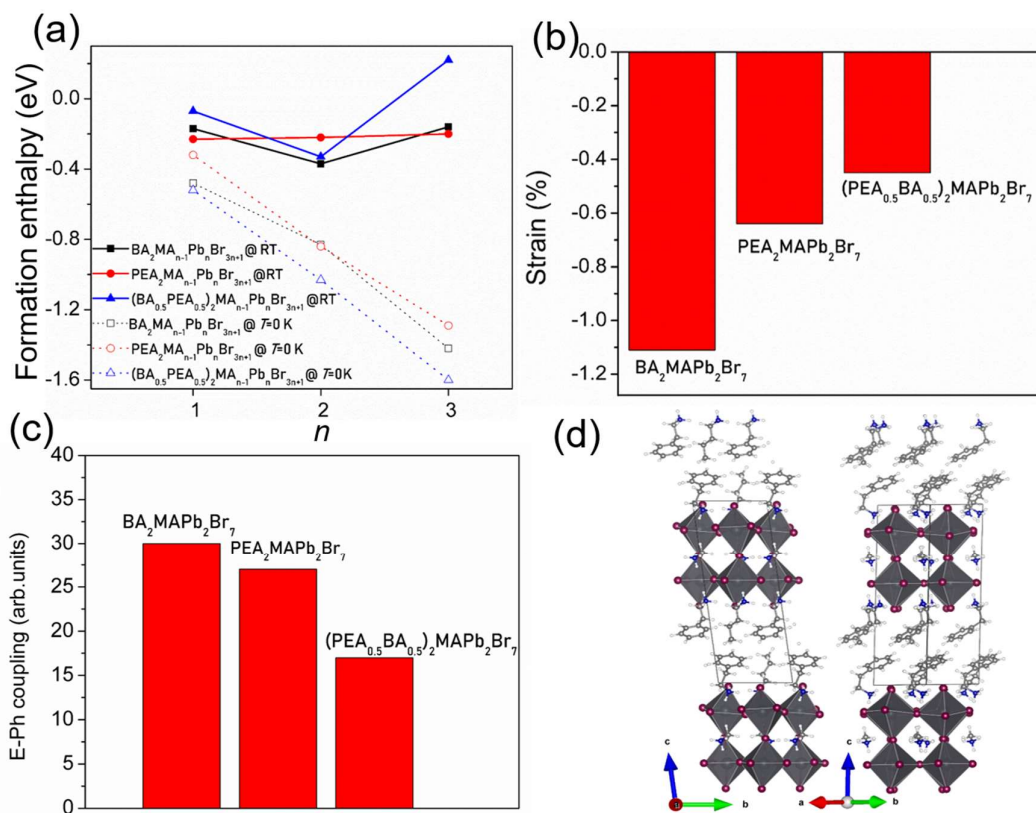[58] G. Bussi, D. Donadio, M. Parrinello, *J. Chem. Phys.* **2007**, *126*, 014101.

Figure 1. a) Formation energies for $BA_2MA_{n-1}Pb_nBr_{3n-1}$, $PEA_2MA_{n-1}Pb_nBr_{3n-1}$ and $(BA_{0.5}PEA_{0.5})_2MA_{n-1}Pb_nBr_{3n-1}$. Full symbols represent energies calculated at RT while the hollow symbols show energies calculated at 0 K. b) Strain for $BA_2MAPb_2Br_7$, $PEA_2MAPb_2Br_7$ and $(BA_{0.5}PEA_{0.5})_2MAPb_2Br_7$ c) E-Ph coupling for $BA_2MAPb_2Br_7$, $PEA_2MAPb_2Br_7$ and $(BA_{0.5}PEA_{0.5})_2MAPb_2Br_7$, d) structure of $(BA_{0.5}PEA_{0.5})_2MAPb_2Br_7$
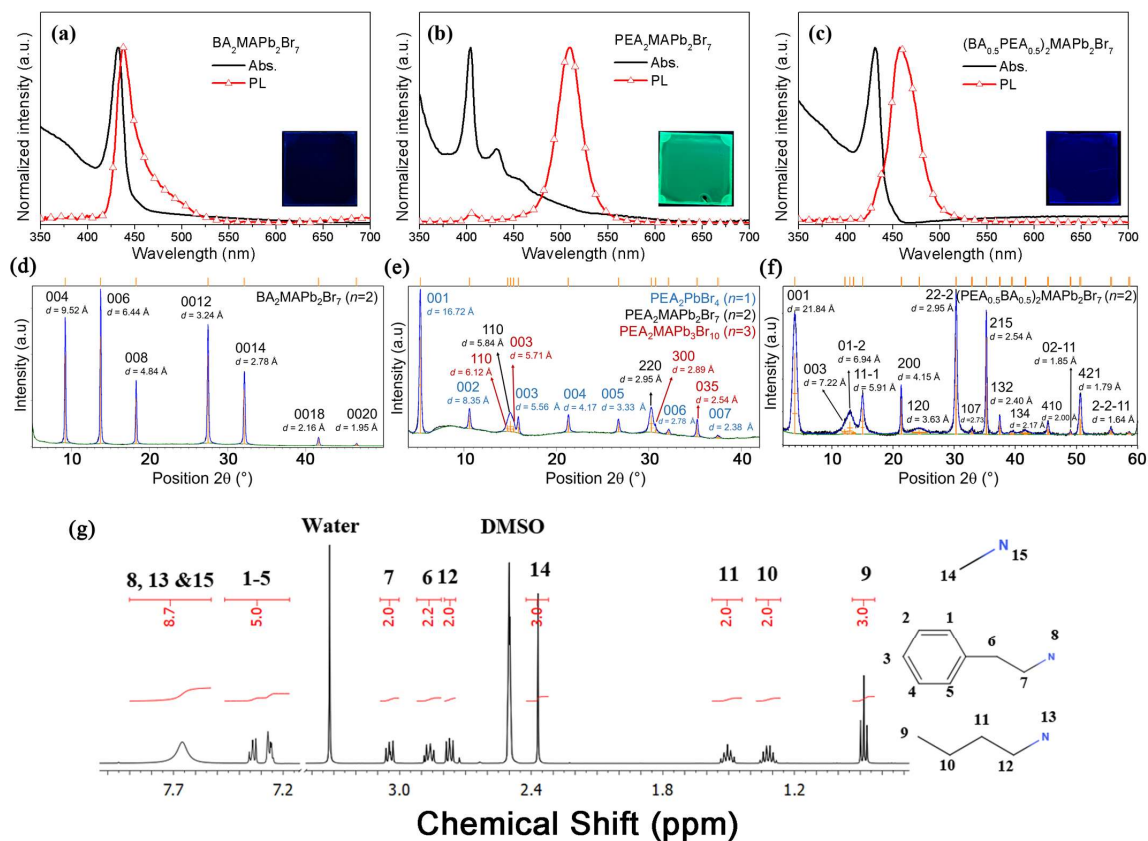
Figure 2. Absorption and PL spectra a) $BA_2MAPb_2Br_7$, b) $PEA_2MA_{n-1}Pb_nBr_{3n+1}$ and c) $(BA_{0.5}PEA_{0.5})_2MAPb_2Br_7$ films prepared with precursor solution of $n=2$ stoichiometr;. XRD patterns of d) $BA_2MAPb_2Br_7$, e) $PEA_2MA_{n-1}Pb_nBr_{3n+1}$, and f) $(BA_{0.5}PEA_{0.5})_2MAPb_2Br_7$ films prepared with precursor solution of $n=2$ stoichiometry; g) H-NMR spectrum of $(BA_{0.5}PEA_{0.5})_2MAPb_2Br_7$ mixed perovskite film dissolved in DMSO-d6. The peaks were assigned with corresponding atoms.
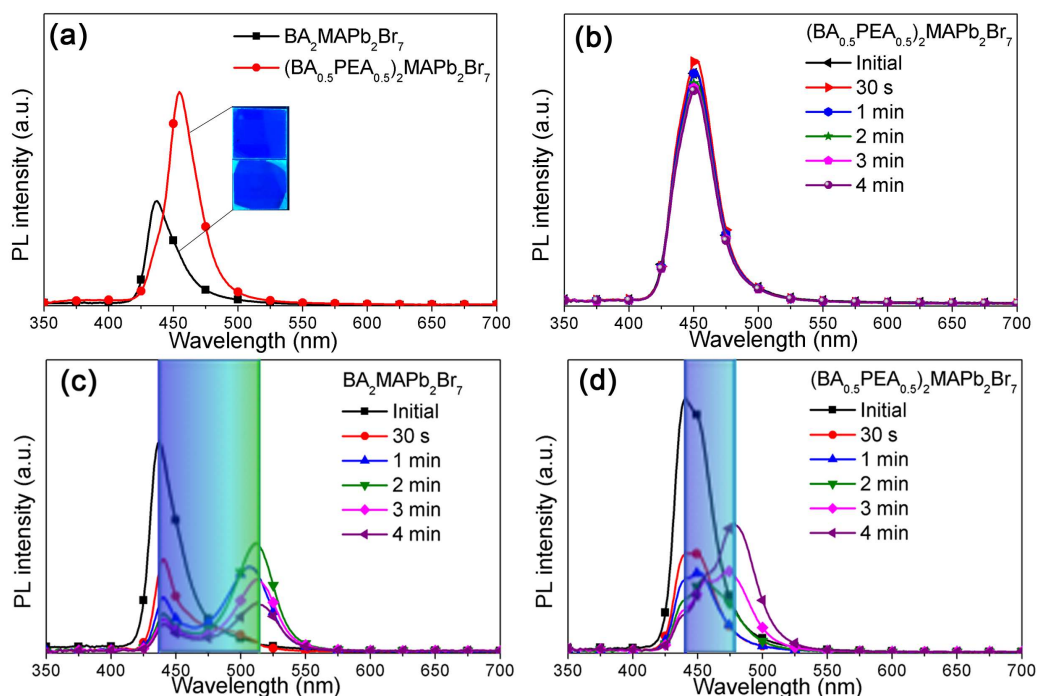
Figure 3. a) PL spectra of $BA_2MAPb_2Br_7$ and $(BA_{0.5}PEA_{0.5})_2MAPb_2Br_7$ thin films with optimized deposition conditions; the inset shows corresponding photos. b) PL spectra of encapsulated $(BA_{0.5}PEA_{0.5})_2MAPb_2Br_7$ films after different durations of laser exposure. PL spectra after different durations of laser exposure in ambient for c) $BA_2MAPb_2Br_7$ and d) $(BA_{0.5}PEA_{0.5})_2MAPb_2Br_7$ films; Corresponding peak colours are indicated.
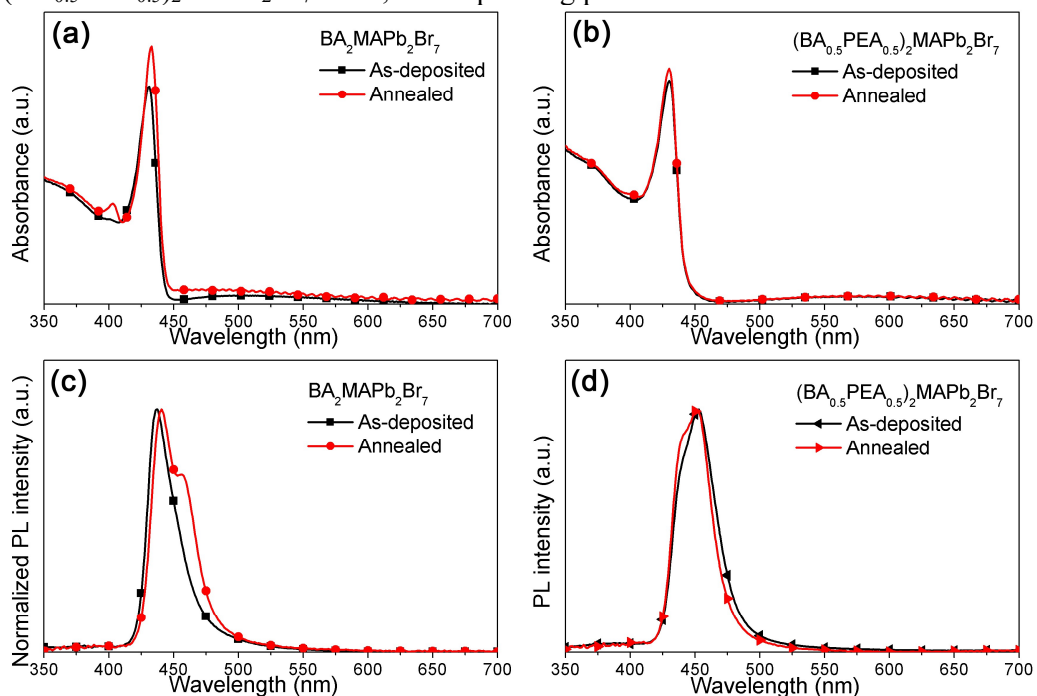
Figure 4. Absorption spectra of as-prepared and annealed samples for a) $BA_2MAPb_2Br_7$ films and b)$(BA_{0.5}PEA_{0.5})_2MAPb_2Br_7$ perovskite films. PL spectra of as-deposited and annealed c) $BA_2MAPb_2Br_7$ and d)$(BA_{0.5}PEA_{0.5})_2MAPb_2Br_7$ films.
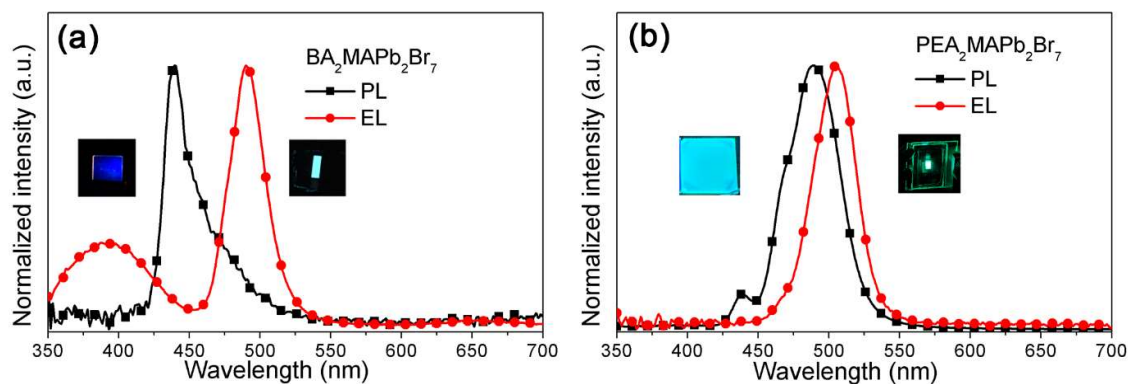
Figure 5. a) Comparison of PL of BA$_2$MAPb$_2$Br$_7$ film, and EL spectra of an LED with BA$_2$MAPb$_2$Br$_7$ which involved temperature increase during LiF deposition for LiF/Al electrode. In the EL spectra, some emission from the charge transport layer can be observed, indicating non-optimized charge transport in the devices in addition to the composition change of the perovskite layer. b) Comparison of PL of PEA$_2$MA$_{n-1}$Pb$_n$Br$_{3n+1}$ (n=2) film prepared with MAc, and EL spectra of an LED with PEA$_2$MA$_{n-1}$Pb$_n$Br$_{3n+1}$ (precursor solution corresponding to n=2 stoichiometry) which involved temperature increase during the deposition Cs$_2$CO$_3$/Al cathode.

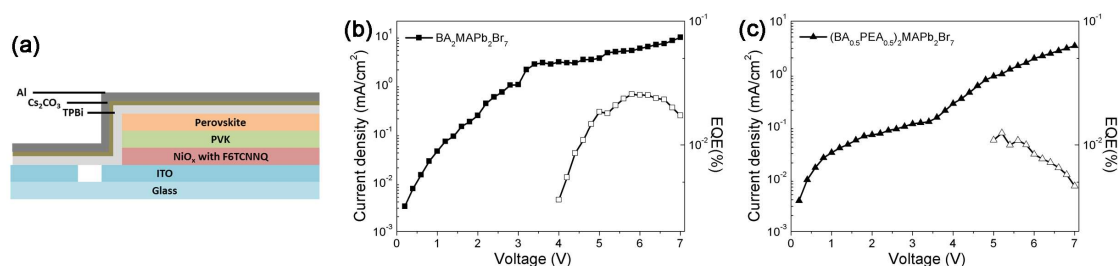**Figure 6.** a) Schematic diagram of LED devices; b, c) I-V and EQE versus voltage bias for BA$_2$MAPb$_2$Br$_7$ and (BA$_{0.5}$PEA$_{0.5}$)$_2$MAPb$_2$Br$_7$ devices, respectively.
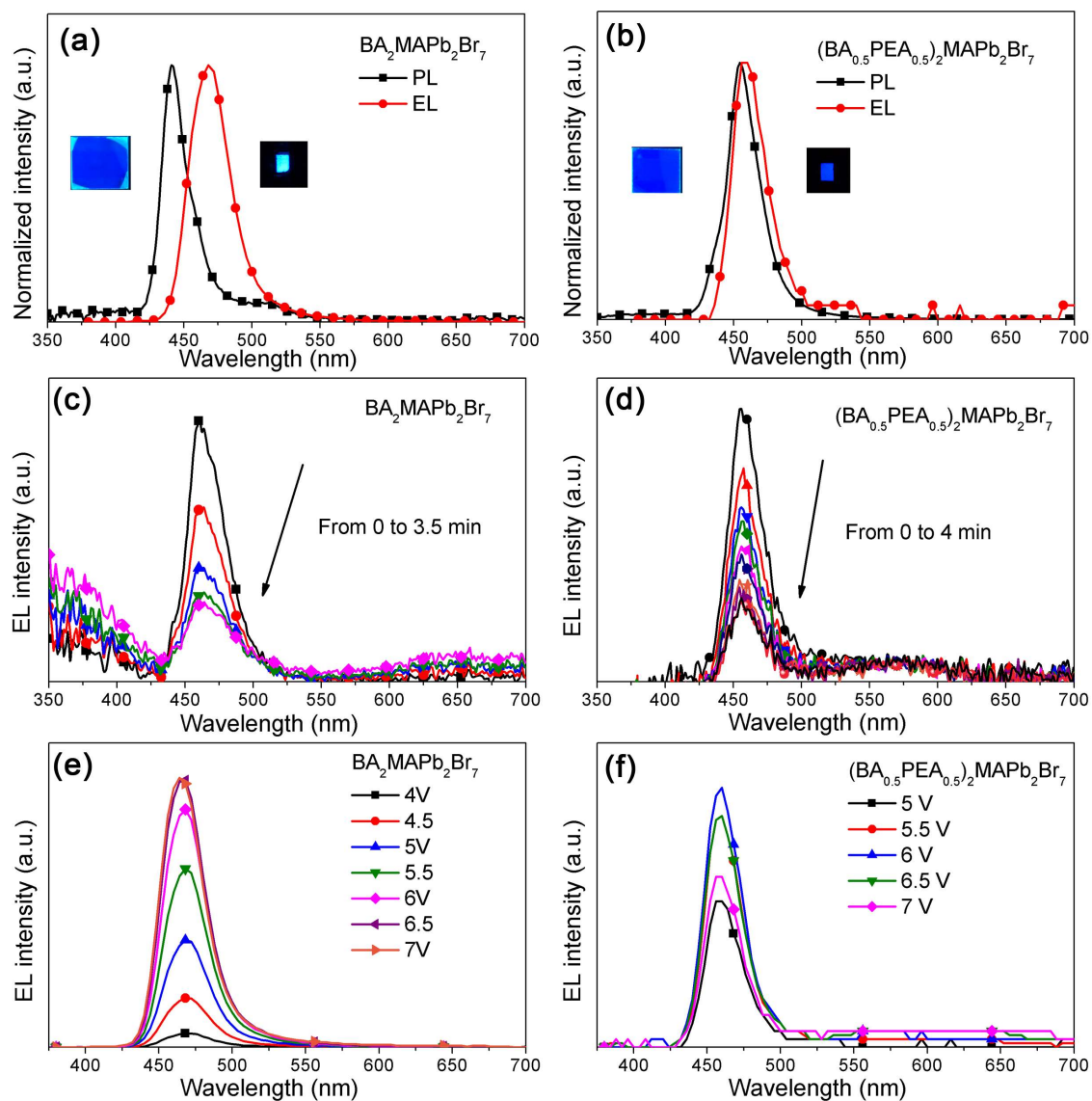
Figure 7. a, b) EL and PL spectra of $BA_2MAPb_2Br_7$ and $(BA_{0.5}PEA_{0.5})_2MAPb_2Br_7$ devices, respectively. The insets show corresponding photos. c, d) EL spectra of $BA_2MAPb_2Br_7$ and $(BA_{0.5}PEA_{0.5})_2MAPb_2Br_7$ devices after different time intervals. e, f) EL spectra of $BA_2MAPb_2Br_7$ and $(BA_{0.5}PEA_{0.5})_2MAPb_2Br_7$ device under different voltage bias.

Ruddlesden-Popper halide perovskite (RPP) materials are promising candidates for light emitting devices with tunable emission wavelength. However, pure blue emission n=2 RPP films are unstable for LED applications. The stabilization of n=2 phase is demonstrated by employing two spacer cations to form a mixed cation bilayer structure. Pure blue LEDs are achieved with excellent spectral stability.

Keyword
Ruddlesden-Popper, quasi-2D perovskites, perovskite light-emitting diodes, blue emission

Tik Lun Leung, Ho Won Tam, Fangzhou Liu, Jingyang Lin, Alan Man Ching Ng, Wai Kin Chan, Wei Chen, Zhubing He, Ivor Lončarić, Luca Grisanti, Chao Ma, Kam Sing Wong, Ying Suet Lau, Furong Zhu, Željko Skoko, Jasminka Popović,* and Aleksandra B. Djurišić*

Mixed spacer cation stabilization of blue-emitting n=2 Ruddlesden-Popper organic-inorganic halide perovskite films

ToC figure